

Inflow and outflow from the accretion disc of the microquasar SS 433: UKIRT spectroscopy

Sebastian Perez M.^{1*} and Katherine M. Blundell¹

¹University of Oxford, Department of Physics, Keble Road, Oxford, OX1 3RH, U.K.

ABSTRACT

A succession of near-IR spectroscopic observations, taken nightly throughout an entire cycle of SS 433’s orbit, reveal (i) the persistent signature of SS 433’s accretion disc, having a rotation speed of $\sim 500 \text{ km s}^{-1}$ (ii) the presence of the circumbinary disc recently discovered at optical wavelengths by Blundell, Bowler & Schmidtobreick (2008) and (iii) a much faster outflow than has previously been measured for the disc wind. From these, we find a much faster accretion disc wind than has noted before, with a terminal velocity of $\sim 1500 \text{ km s}^{-1}$. The increased wind terminal velocity results in a mass-loss rate of $\sim 10^{-4} M_{\odot} \text{ yr}^{-1}$. These, together with the newly (upwardly) determined masses for the components of the SS 433 system, result in an accurate diagnosis of the extent to which SS 433 has super-Eddington flows. Our observations imply that the size of the companion star is comparable with the semi-minor axis of the orbit which is given by $\sqrt{1 - e^2} 40 R_{\odot}$, where e is the eccentricity. Our relatively high spectral resolution at these near-IR wavelengths has enabled us to deconstruct the different components that comprise the Brackett- γ line in this binary system, and their physical origins. With this line dominated throughout our series of observations by the disc wind, and the accretion disc itself being only a minority (~ 15 per cent) contribution, we caution against use of the unresolved Brackett- γ line intensity as an “accretion signature” in X-ray binaries or microquasars in any quantitative way.

Key words: accretion, accretion discs – stars: individual: SS 433 – stars: winds, outflows – binaries: spectroscopic

1 INTRODUCTION

SS 433, named in 1977 as Stephenson and Sanduleak’s 433rd entry in their catalogue of $\text{H}\alpha$ emitters, was first recognised as an X-ray and radio source by Clark & Murdin (1978), possibly associated with the supernova remnant W50. It became famous as the first known relativistic jet source in the Galaxy, and is the only one known with baryonic content in its jets (see comprehensive review by Fabrika 2004). Its jets are believed to emerge from an accretion disc, but direct evidence for this has thus far been scant.

The mass of the system has been elusive over the last 30 years. For example, Hillwig & Gies (2008), from observations of absorption lines, reported masses of ~ 12 and $\sim 4 M_{\odot}$ for the donor star and the compact object, respectively. On the other hand, D’Odorico et al. (1991) had previously suggested that the masses of the components were rather low, $\sim 3.2 M_{\odot}$ and $\sim 0.8 M_{\odot}$ for the donor and the compact object, respectively. Lopez et al. (2006), looking at the eclipses seen in X-ray spectra, suggested masses of ~ 35 and $\sim 20 M_{\odot}$ for the donor and the compact object, respectively. Recent analysis of the stationary $\text{H}\alpha$ line has shown, from

dynamical considerations, that the enclosed mass for the whole system is quite large, around $40 M_{\odot}$, and that the mass for the compact object plus accretion disc attains $16 M_{\odot}$, therefore also implying that the identity of the compact object is a rather massive stellar black hole (Blundell et al. 2008).

At near-infrared wavelengths, SS 433 is characterised by a red continuum and bright emission lines (Thompson et al. 1979; McAlary & McLaren 1980). As at optical and X-ray wavelengths, these emission lines can be divided into two groups: (a) *stationary* lines, although highly variable in strength and profile shape; (b) *moving* lines, thought to originate in two oppositely-directed relativistic jets of baryonic content (moving with speed $v \sim 0.26 c$). The stationary emission lines are thought to be produced in the accretion flow and in an expanding, geometrically thick environment fed from the stellar wind and the super-Eddington accretion disc outflow (Gies et al. 2002; Fabrika 2004).

The system shows three main periodicities: the binary’s orbital motion, with a period of about 13.1 days (Crampton & Hutchings 1981); and the jet axis’s precession and nutation, with periods of about 162 and 6 days, respectively. A configuration where the jet axis undergoes a precession cycle in 162 days, referred as the *kinematical model*, was proposed to describe the motion of the lines

* E-mail: s.perez2@physics.ox.ac.uk

(Fabian & Rees 1979; Milgrom 1979). In order to account for the 6-day nodding cycle, Katz et al. (1982) proposed a dynamical model where the companion exerts a gravitational torque on the disc periphery.

Near-IR light can escape high opacity and dusty environments more easily than $H\alpha$ photons can, making it possible to detect heavily obscured line-emitting regions. We carried out a line deblending procedure based on fitting Gaussian profiles to our near-IR spectra, choosing Brackett- γ (hereafter $Br\gamma$) at $\lambda 2.165 \mu\text{m}$ as the most suitable emission line to model.

The $Br\gamma$ recombination line has been extensively used in the past to diagnose the presence of accretion discs and outflows (e.g., Bandyopadhyay et al. 1997; Shahbaz et al. 1999). In the case of cataclysmic variables (CVs), Dhillon & Marsh (1995) argued that since the Brackett and He I emission lines are so strong in emission and also so broad that they must originate in the accretion disc. In low-mass X-ray binaries (LMXBs) the $Br\gamma$ line has been detected showing a double-peaked profile characteristic of accretion discs. Bandyopadhyay et al. (1997) used the distance between the peaks to calculate properties of the orbits in LMXBs, assuming that the compact object accretes via Roche-lobe overflow.

In this work, we present unprecedentedly high signal-to-noise mid-resolution near-IR spectra of SS 433 from UKIRT that has enabled us to identify the accretion disc and its outflow. In Section 2, we begin by giving a brief description of the UKIRT observations and the data reduction. In Section 3 we discuss the results of deconstructing the $Br\gamma$ emission line in order to identify and quantify the different components present in emission in the system throughout an orbital period. Finally we discuss and give concluding remarks on this work in Sections 4 and 5.

2 OBSERVATIONS AND DATA REDUCTION

We observed SS 433 every night over an entire orbital cycle with the UKIRT UIST spectrograph (Ramsay Howat et al. 2004) from 2006 August 17 to August 29, during which time the precession phase varied from 0.40 to 0.47 respectively. We use the convention in which orbital phase (ϕ_{orb}) zero is when the donor star is eclipsing out the compact object (Goranskii et al. 1998). Precessional phases (ψ_{pre}) are based on the ephemeris reported in Fabrika (2004), where precession phase zero is when the jet lines are maximally separated hence the inclination of the jet axis with our line-of-sight attains a minimum, i.e., it corresponds to maximum exposure of the accretion disc to the observer.

UIST is a 1–5 μm imager-spectrometer with a 1024×1024 InSb array. The plate scale in spectroscopic mode is $0''.12 \text{ pixel}^{-1}$. We used a slit of width $0''.24$. The spectral resolution $R = \lambda/\Delta\lambda$ is about 4000 for the J -band and 3900 for the K -band. The top of the slit was pointing to the east and centred on SS 433's optical position during acquisition. There were no problems in acquiring the target since SS 433 is a very bright red object with $K \sim 8$ mag. Our data consist of 13 nights of K -band high-resolution spectra and one night, at primary minimum, covering the complete near-IR window (J , H and K -bands).

The observing strategy consisted of taking about forty frames with exposure times of 45 s each, following an ABBA nodding pattern. The pixel-to-pixel response of the array was corrected using the normalised, reduced flat field. Bad pixels, correction of detector defects and cosmic-ray removal were performed using standard median filtering techniques. Frequent observations of a standard star (BS6697) and the arc lamp were performed during each night

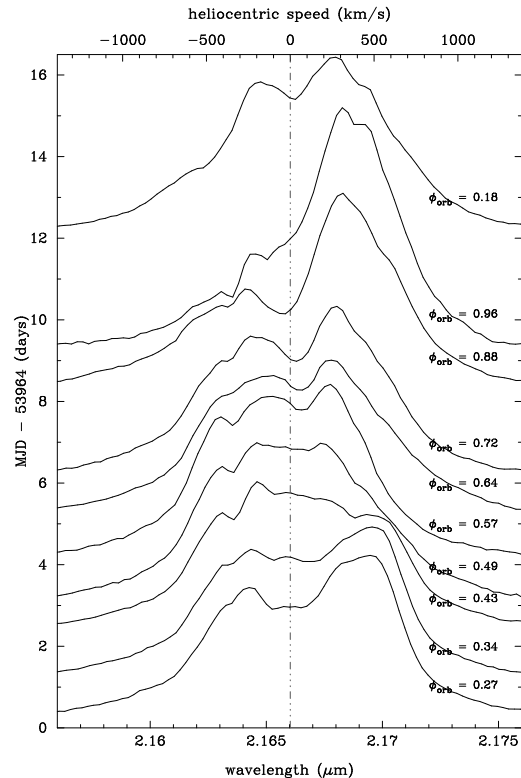


Figure 1. Individual $Br\gamma$ stationary profiles plotted as a function of wavelength and modified Julian date of observation. Their continua are normalised to unity and aligned with the mean day of their observation. Each spectrum is labelled with its orbital phase on the right hand side. The dashed line corresponds to the systemic velocity measured from the Mg II radial velocity curve (Perez et al. *in prep*).

to provide an accurate estimate of the wavelength axis. Wavelength calibration was carried out by fitting a high-order polynomial to the Argon lamp arc spectra, taken each night. In order to remove the sky contribution, pairs of nodded frames were subtracted. Standard star division was applied to each frame in order to flux calibrate the data. The intrinsic photospheric features were carefully removed from the standard star by interpolating or fitting a Voigt profile when needed. Great care was taken to cancel the telluric features, especially the CO_2 absorption near $2.05 \mu\text{m}$. Finally, the spectra were extracted using Horne's optimal extraction algorithm (Horne 1986) and then combined to produce an average spectrum for each night with an exposure time of about 2 ks giving a signal-to-noise ~ 400 in the $Br\gamma$ line.

All data reduction and analysis were carried out using the Perl Data Language.¹ The reduced spectra centred on the heliocentric $Br\gamma$ line are displayed in Fig. 1 from which it is immediately apparent that there is considerable structure in this emission line, and considerable variation of this structure. We deconstruct these structures in the next section.

3 DECONSTRUCTING THE BRACKETT- γ PROFILE

Many other authors have studied the stationary $H\alpha$ line profile in detail (e.g., Falomo et al. 1987; Gies et al. 2002), albeit over

¹ <http://pdl.perl.org>.

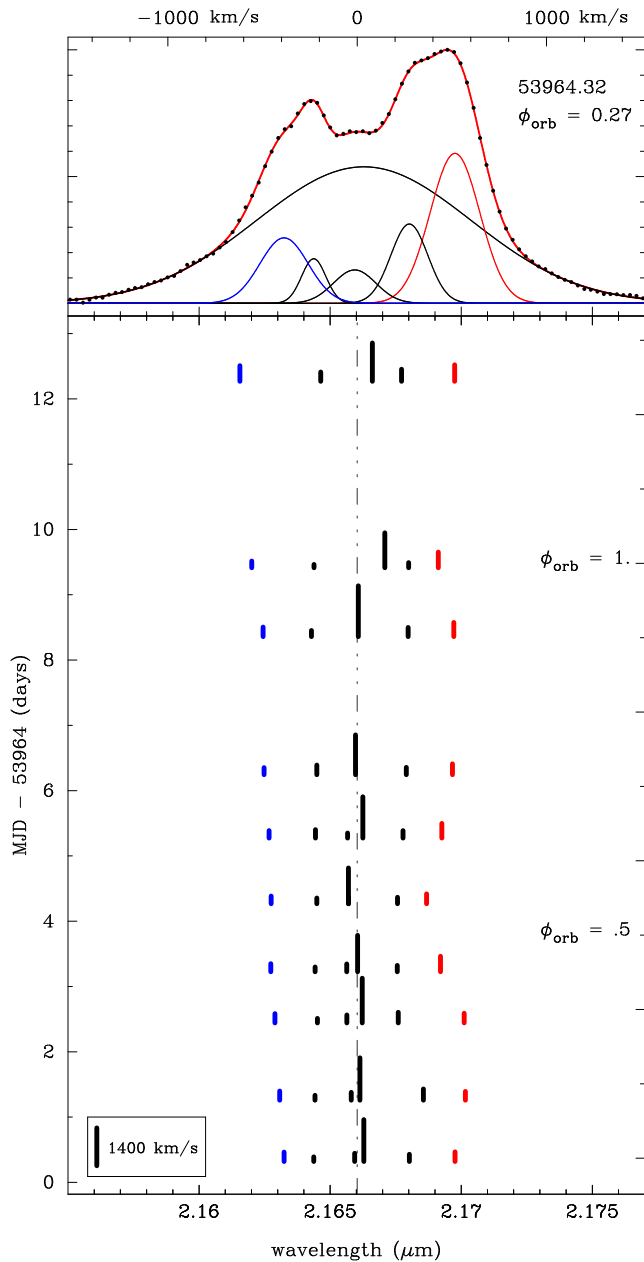


Figure 2. *Upper panel:* Example of Br γ stationary emission lines observed at orbital phase $\phi_{\text{orb}} = 0.27$; the top x -axis corresponds to heliocentric speed in units of km s^{-1} . *Lower panel:* Tracks of the centroids of the Gaussian components fitted to each of our spectra. The modified Julian date (MJD) increases vertically and the tick mark heights are proportional to the FWHM of each component (see inset in the bottom left corner).

rather shorter observing runs. Decomposition of a line profile as the sum of Gaussian components is a technique widely used to extract information from different parcels of gas in a line emitting region. For example, in the case of Seyfert galaxies it allows one to distinguish the narrow line region from the broad line region (e.g., Ho et al. 1997). Blundell et al. (2008) decomposed the stationary H α line (observed during a quiescent period in SS 433’s behaviour) into primarily 3 components: one broad component (FWHM $\sim 700 \text{ km s}^{-1}$) whose width was observed to decrease with precessional phase (i.e., as the jets become more in the plane of the sky) identified as the accretion disc wind, and two narrower, red-

and blue-shifted components, but stationary in wavelength, being radiated from a glowing circumbinary ring.

The stationary Br γ emission lines show a much more complex profile than the quiescent H α line studied by Blundell et al. (2008). After trying with different numbers of Gaussian components we came to the realisation that up to six components were needed to account for the complexity of the Br γ profile shape. Fig. 2 (upper panel) shows an example of a fitted Br γ profile; in this case six Gaussians were used in the fit.

The presence of a P Cygni feature in the stationary lines has been noted by several authors at certain precessional phases (Crampton & Hutchings 1981; Filippenko et al. 1988; Gies et al. 2002). An absorption feature in the blue wing of the line profile would indeed complicate the analysis and it would have to be taken into account using models of outflowing winds (e.g., Castor & Lamers 1979). However, we have found no clear evidence of the presence of such absorption feature at the epochs at which we observed SS 433 (see e.g., top panel of Fig. 2).

Fig. 2 (lower panel) shows the components of the stationary Br γ line as a function of time. It is easy to see that the Br γ complex can be decomposed in three main constituents: a very broad wind component present at all times in our data-set and two sets of narrower pairs. The broad wind and both narrower pairs show a mean velocity close to the systemic speed $V_0 \simeq 150 \text{ km s}^{-1}$ (see lower panel in Fig. 3). This measurement of the systemic velocity was obtained from the radial velocity curve of the Mg II $\lambda 2.404 \mu\text{m}$ stationary line (Perez et al. *in prep*). Although this value seems to fit well with all the stationary emission lines in our near-IR spectra, it is very different compared to other previous observations (e.g., 27 km s^{-1} by Crampton & Hutchings (1981), 73 km s^{-1} by Hillwig & Gies (2008) and -44 km s^{-1} by Gies et al. (2002)).

The broad components plotted in Fig. 2 show FWHMs from 1300 up to 1500 km s^{-1} . The presence of a broad wind component has been reported before from H α stationary line analysis but with FWHM reaching only up to 800 km s^{-1} (Falomo et al. 1987) and 700 km s^{-1} during the quiescent period reported by Blundell et al. (2008), although broader widths have been observed before and during a flare by Blundell et al. *in prep*.

The inner set of narrow lines, moving at speeds $\sim 200 \text{ km s}^{-1}$, are fairly steady in wavelength, in excellent agreement with the presence of a circumbinary ring reported by Blundell et al. (2008).

The most striking discovery that arises from the Br γ line fitting is the presence of a pair of widely-separated, hence rapidly rotating, narrow components. An example of these narrow (but widely separated) pairs are depicted in red and blue colours in the upper panel of Fig. 2. The speed with which the radiating material spirals in the accretion disc corresponds to half the difference of the speed of those lines, under the assumption that the fitted centroids correspond to the tangent speed. This reveals material that is spiralling in the potential well at speeds of about 500 km s^{-1} (see upper panel in Fig. 3). The accretion disc lines also show a somewhat sinusoidal variation, as can be seen in Fig. 3, with a peak-to-peak amplitude of $\sim 100 \text{ km s}^{-1}$.

The sixth component, that only appears between $\phi_{\text{orb}} = 0.2$ and 0.6, seen in Fig. 2 as a small Gaussian blueward of the position of the broad wind, may correspond to much more extended line emission that is somehow bonded to the system, hence it moves at about the systemic velocity but it does not obviously show any of the characteristic periodicities.

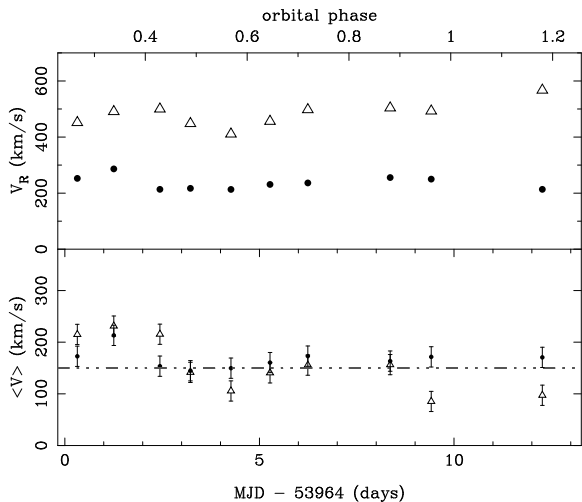


Figure 3. Rotational (upper) and mean (lower) speeds of the rapidly rotating components in the $\text{Br}\gamma$ line. Open triangles correspond to the widely (500 km s^{-1}) separated disc lines, while solid circles correspond to the circumbinary ring lines. The rotational speed is calculated from half the difference of the redshifts of the red and blue components in Fig 2. Symbol sizes correspond to 1σ error bars.

4 DISCUSSION

4.1 The accretion disc and its persistent appearance in the near-IR

Fleeting glimpses of widely separated pairs of lines centred on $\text{H}\alpha$ have been observed very briefly by Falomo et al. (1987), and immediately prior to a flare by Blundell et al. *in prep*, implying a high rotation speed. It is remarkable that the lines having a rotation speed of 500 km s^{-1} seem to be persistent in near-IR observations, rather than fleeting or associated with flares as in the optical: we have no reason to believe that any of our near-IR observations were during, or just before, a flare.² Moreover, other near-IR observations, both our own in H -band observations of Brackett- ζ $1.74 \mu\text{m}$ and archival CGS4 observations, are consistent with the presence of a pair of lines whose positions correspond to a rotation speed of $\gtrsim 500 \text{ km s}^{-1}$. These are depicted in Fig. 4. For a test particle to move with a Keplerian velocity of $\sim 500 \text{ km s}^{-1}$ around an object with a mass of $\sim 16 M_{\odot}$ (as estimated by Blundell et al. 2008) it would have to be located at approximately $12 R_{\odot}$ away from the central object. This gives us an idea of the extent of the accretion disc.

Several authors have utilised hydrogenic lines to study accreting systems (e.g., Bandyopadhyay et al. 1997; Shahbaz et al. 1999). From observations of low-mass X-ray binaries, Bandyopadhyay et al. (1999) have revealed the presence of outflows and winds in some accreting mass objects. We emphasise the fact that using the $\text{Br}\gamma$ line as a signature of accretion has to be undertaken with care since the $\text{Br}\gamma$ emission is telling us about outflow via various means, not merely accretion inflow onto a compact object.

The area of each accretion disc line (i.e., the components moving at $\sim 500 \text{ km s}^{-1}$) seems to be correlated: the difference between the areas of these two lines shows a very clear orbital phase

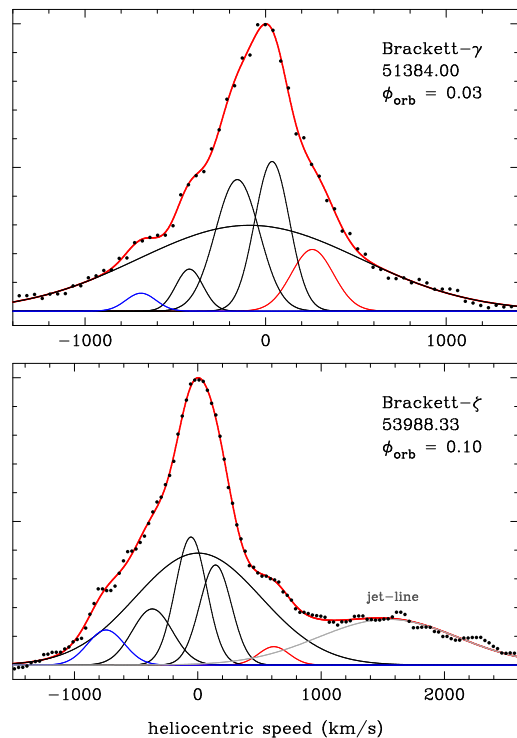


Figure 4. *Upper panel:* Archival CSG4 spectrum of $\text{Br}\gamma$ stationary line taken on 1999 July 25 at orbital phase $\phi_{\text{orb}} = 0.03$ as a function of heliocentric speed in units of km s^{-1} . *Lower panel:* Brackett- ζ spectrum taken on the last night of our observing run (2006 September 10) at orbital phase $\phi_{\text{orb}} = 0.1$ as a function of heliocentric speed. Both observations correspond to precessional phase ~ 0.5 . The modified Julian day of each observation is specified on each plot.

dependence (see panel 1a in Fig. 5). As we can see in panel 2b of Fig. 5 the FWHM of each line does not show periodic variations, it is around 300 km s^{-1} with a scatter of $\sim 70 \text{ km s}^{-1}$. On the other hand, panel 3a of the same figure shows that the HEIGHT of each line clearly depends on orbital phase. This behaviour is what we would expect if the material emitting these components comes from the disc, because as the star, together with the spherically symmetric wind/corona, transits in front of the disc it partially obscures the emitting regions.

The crucial points of the orbital phase dependence are as follows: (i) at orbital phase 0.5, the compact object and its accretion disc are closer along our line of sight than the companion star is — at this orbital phase there is no asymmetric obscuration so there is zero difference in the areas of the red and blue lines. (ii) At all other orbital phases, the red line area (and indeed height) exceeds that of the blue line. From this we draw two conclusions: first there is low level obscuration from the stellar wind at all orbital phases except when the disc acts as its own windbreak at orbital phase 0.5. (We note that most of the time SS 433’s accretion disc is completely obscured in the optical.) At all other phases besides 0.5 there is a component of the stellar wind between us and the disc lines that attenuates the blue lines somewhat more than the red lines. Second, we conclude that the sinusoidal variation in area difference does indeed tell us about the radial extent of the surface of the star, or of its obscuring stellar wind. The maximal difference in area occurs at orbital phase 1.0 when the star is closer along our line of sight than the accretion disc and compact object: this is the phase when the greatest attenuating path length though the star (or its dense stellar

² We checked the radio monitoring records of the Ryle telescope (Guy Pooley) and the RATAN telescope (Sergei Trushkin).

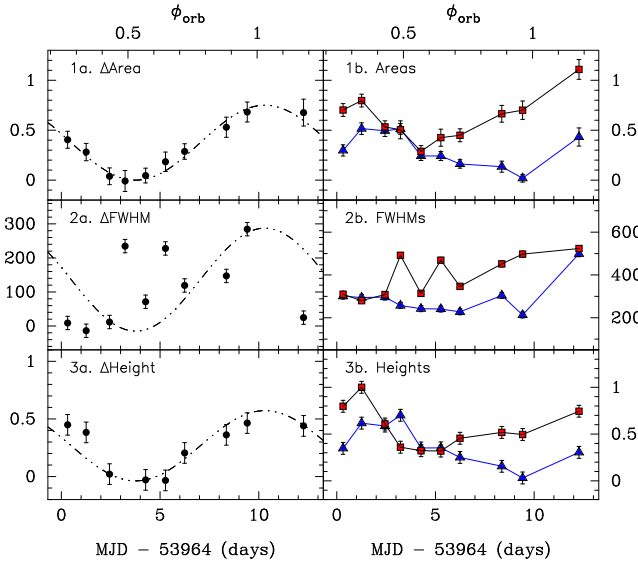


Figure 5. Panel 1a: Difference between the areas of the two widely-separated (500 km s^{-1}) components, red- minus blue-shifted (the y-axis is in units of $10^{-15} \text{ W m}^{-2}$). Notice the orbital phase dependence (the dashed line is the sinusoidal variation corresponding to that orbital phase). **Panel 1b:** Areas of red and blue accretion disc lines as a function of time. **Panels 2a and 2b** are the same as in the upper panel but for the FWHM (in km s^{-1}) of each accretion disc line. **Panels 3a and 3b** are the equivalent plots for the HEIGHTS of the Gaussians fitted to the red and blue components, in units of $1.6 \times 10^{-13} \text{ W m}^{-2} \mu\text{m}^{-1}$. Error bars correspond to 1σ uncertainties.

wind) is presented from the accretion disc along the line of sight to Earth. The fact that the variation is sinusoidal is consistent with a reasonably circularly (spherically) symmetric stellar wind.

4.1.1 Implications for the geometry of the system

In the previous sub-section we found that the companion star (and its wind) eclipses out some areas of the accretion disc. If the orbit of the system is essentially circular then the variation of the difference of the accretion disc's lines (Fig. 5) implies that the star has a diameter comparable with the radius of the orbit. On the other hand, if the orbit is rather elliptical, then the star is smaller and the semi-major axis of the orbit must be along our line-of-sight as inferred from the shape of the light curve, namely, the fact that the secondary minima occurs precisely close to mid-way between the primary minima (see eg., Kemp et al. 1986; Goranskii et al. 1998).

Recently, Blundell et al. (2008) found that the total mass of SS 433 is approximately $40 M_{\odot}$. We can roughly estimate the size of the system to be about twice the semi-major axis of the orbit a , as given by Kepler's third law: $a^3 = GM_{\text{sys}}(P_{\text{orb}}/2\pi)^2$, where P_{orb} is the orbital period and M_{sys} is the total mass of the binary. This relation implies a size for the whole system of $2a \simeq 160 R_{\odot}$. The radius of the companion star should be $R \sim a/2$. Thus, the eclipsing of the widely-separated accretion disc lines implies a maximum radius for the companion star $R \simeq 40 R_{\odot}$. For other recent mass estimates we obtain similarly large values for the size of the star: Hillwig & Gies (2008) reported $M_{\text{sys}} \approx 16 M_{\odot}$ implying $R \sim 29 R_{\odot}$ and Lopez et al. (2006) estimated $M_{\text{sys}} \approx 55 M_{\odot}$ which yields $R \sim 44 R_{\odot}$. All of these mass estimates assume the case where the orbit is essentially circular. This size is smaller but still comparable with the radius of evolved stars undergoing severe

mass-loss such as $\eta \text{ Car}$ ($\sim 80 R_{\odot}$). This large size is reduced only at the expense of accepting an eccentric orbit. The size of the companion star in the eccentric case would be $b = \sqrt{1 - e^2} 40 R_{\odot}$ where b is the semi-minor axis of the orbit and e is the eccentricity.

4.2 The disc wind: near-IR view and mass-loss rate

4.2.1 Precessional- and orbital-phase dependence, or lack thereof

Fig. 2 shows that the broad wind component, inferred (on the basis of optical observations, Blundell et al. 2008) to originate from the disc, lacks indications of orbital and nutational periodicities manifested by the accretion disc. We have not been able to test for precessional phase dependence due to our observations spanning only 0.07 of a precessional phase. A possible explanation of this could be that the near-IR wind comes from very close into the centre of the disc, where the temperature of the gas could reach $\sim 10^8 \text{ K}$. At these small radii the material only experiences the influence of the compact object and any tidal torque from the companion star could be a negligible perturbation. At greater radii as observable in the optical, the torques exerted by the companion are much stronger, hence precessional periodicities are manifested.

4.2.2 Mass-loss via line-driven winds

Close binary systems undergo severe mass loss and mass exchange during their lifetime. Like early-type stars, their spectra show a number of emission lines due to the large amount of ionised gas present in the system. This ionised gas produces thermal radio emission and an excess of continuum photons at infra-red wavelengths, which somewhat correlates with line emission, yielding similar mass loss estimates. These three spectral features yield mass-loss rate estimates for emission line stars (Kogure & Leung 2007).

Leitherer (1988) has used the luminosity of the optically-thin $H\alpha$ line as a mass-loss tracer. The relation between \dot{M} and luminosity relies on the dependence of both quantities on the density of the wind, $\rho(r)$. Following Leitherer's approach we can derive an equivalent expression for $\text{Br}\gamma$ emission, by assuming that the emission is optically thin in an isothermal wind. Therefore, the luminosity of a recombination line, L_l , will be given by:

$$L_l = C_n f(T_{\text{eff}}) I(v_0/v_{\infty}, \beta) \frac{\dot{M}^2}{\mu^2 v_{\infty}^2 R}, \quad (1)$$

where v_{∞} is the terminal speed reached by the wind, μ is the mean atomic weight and R is the radius of the source (i.e., where the wind starts), \dot{M} is the mass-loss rate, I is an integral defined below and β is a parameter that controls the shape of the velocity law of the wind. C_n and $f(T_{\text{eff}})$ are constants for each transition given by:

$$C_n = \frac{n_1^2 A_{12} h \nu_{12}}{4\pi m_{\text{H}}^2} \left(\frac{h^2}{2\pi m_e k} \right)^{3/2}, \quad (2)$$

and,

$$f(T_{\text{eff}}) = b_n T_e^{-3/2} e^{\chi_n/kT_e}, \quad (3)$$

where n_1 and n_2 are the principal quantum numbers corresponding to the upper and lower levels in the atom, respectively. The parameter b_n denotes the departure coefficient and it accounts for non-LTE effects (assumed to be ~ 1 for simplicity). A_{12} is the transition probability, k is the Boltzmann constant and χ_n is the ionisation potential of the level n_1 . We assume that the wind regions are in

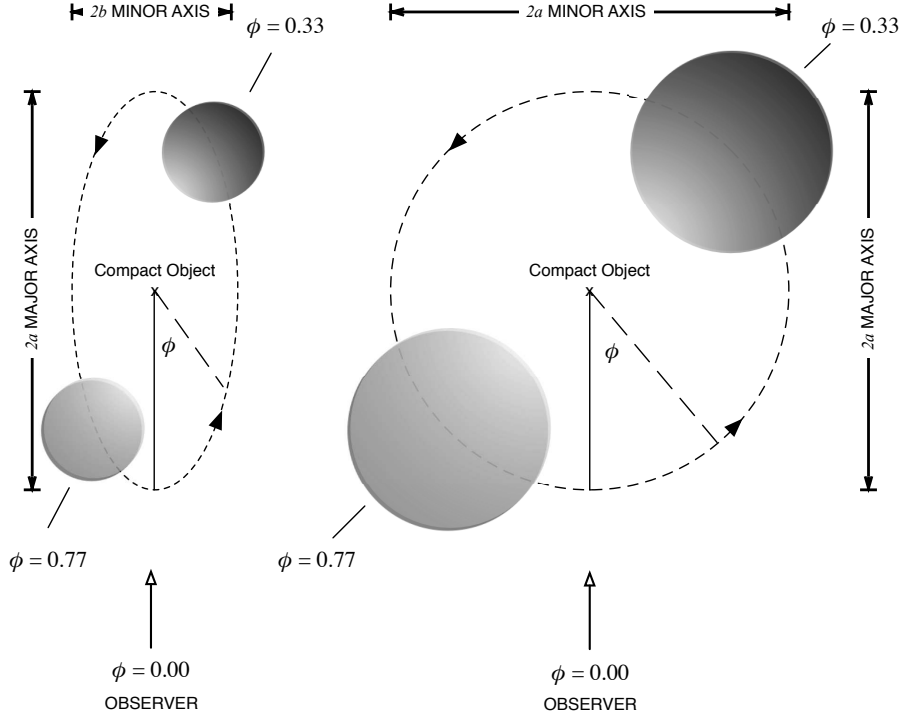


Figure 6. Diagram that shows the 2 possible extreme scenarios concerning the configuration of the SS 433 binary system: (left) eccentric orbit, (right) circular orbit. The semi-major axis of the orbit is $a \simeq 80 R_{\odot}$ (see Section 4.1.1).

radiative equilibrium, i.e., the system's effective temperature T_{eff} is very close to the electron temperature, T_e .

The quantity $I = I(v_0/v_{\infty}, \beta)$ in equation 1 represents the integral over the ratio between the dilution factor and the square of the velocity law $v(r)$. In the case where the velocity law corresponds to a β -law proposed by Castor & Lamers (1979) and the dilution factor is the standard formula given by Kogure & Leung (2007), the integral is given by:

$$I = \frac{1}{2} \int_0^1 \frac{1 - \sqrt{1 - x^2}}{[u + (1 - u)(1 - x)^{\beta}]^2} dx, \quad (4)$$

where $x = R/r$, r being the distance from the centre of the source, and $u = v_0/v_{\infty}$. The speed v_0 is the initial velocity of the wind at $r = R$.

4.2.3 Mass-loss rate via the disc wind

During our observations, the wind Br γ luminosity attains a maximum at $\phi_{\text{orb}} = 0.5$, supporting the idea that this emission comes from the accretion disc; we have measured this flux density to be $F(\text{Br}\gamma) = (6 \pm 0.5) \times 10^{-15} \text{ W m}^{-2}$. The distance to SS 433 has been accurately determined by Blundell & Bowler (2004) as $d = 5.5 \pm 0.2 \text{ kpc}$. This yields a luminosity for the wind in Br γ of $14 \pm 1 L_{\odot}$ (corrected for $A_v = 7.8$ magnitudes of optical extinction). We expect the wind to start at least at a radius $R = 20 R_{\odot}$ from the compact object, according to the dimensions of the system (see Fig. 6). We computed the integral in equation 4 assuming an exponent $\beta \approx 0.7$ and an initial velocity of the order of the sound speed $v_0 = 15 \text{ km s}^{-1}$ (or $0.01 v_{\infty}$), which is a good approximation for hot early-type stars (Leitherer 1988). Because of severe dust extinction towards SS 433 there are no measurements of the terminal velocity from UV P-Cygni profiles. Therefore we use the

width of the wind component $\text{FWHM} \simeq 1500 \text{ km s}^{-1}$ as the terminal velocity of the wind. This is a very modest value compared with some early-type stars (Leitherer 1988). The effective temperature has been estimated to be $T_{\text{eff}} = 5 \times 10^4 \text{ K}$ by fitting the optical-UV spectral flux distribution (Gies et al. 2002). The mean atomic weight of evolved massive stars is $\mu \approx 2$ (Fuchs et al. 2006).

If we apply equation 1 to the Br γ transition of hydrogen (i.e., $n_1 = 7$ and $n_2 = 4$) we find a useful formula that relates the mass loss with the luminosity of the wind:

$$\dot{M}_{\text{wind}} \simeq 1 \times 10^{-4} M_{\odot} \text{ yr}^{-1} \times \mu_2 v_{1500} R_{20}^{1/2} L_{10}^{1/2}, \quad (5)$$

where $\mu_2 = \mu/2$, $v_{1500} = v_{\infty}/1500 \text{ km s}^{-1}$, $R_{20} = R/20 R_{\odot}$ and $L_{10} = L(\text{Br}\gamma)/10 L_{\odot}$.

This value is the same order of magnitude as the mass-loss rate estimated by Fuchs et al. (2006) who fitted the mid-IR continuum. These estimates, although discrepant by a factor of 2–3, are in reasonably good agreement given that both approaches may suffer from the assumptions made regarding the geometry of the system and the choice of some physical parameters. A crucial unknown is the mean atomic weight of the wind, since the mass-loss ratio scales with μ as $\dot{M} \propto \mu$. Leitherer et al. (1995) studied the composition of early-type stars and from the H/He ratios they inferred values for μ between 1.5 and 2.7. Another important source of uncertainty is the choice of velocity law. For $\beta < 1$ the mass-loss rate scales at most by a factor of 2 and it is quite insensitive to the choice of v_0 . On the other hand, for values of β greater than one, \dot{M} depends heavily upon v_0 . Fortunately, $\beta \simeq 0.7 - 0.8$ for winds in O-stars which may match SS 433's hot environment better than B or colder stars (which have $\beta > 1$). The final important effect that must be taken into account is the clumpiness of the wind. Lenorzer et al. (2004) show that the Br γ line may be especially affected by inhomogeneities in the wind. An unclumped wind density can be taken

as the real wind density multiplied by a *clumpiness* factor f . Thus, when clumpiness is present in the wind \dot{M} is reduced by a factor \sqrt{f} (Lenorzer et al. 2004). However, the degree of clumpiness is not very high closer to the source where the Br γ line is formed, thus it should not dramatically affect our estimates.

Although continuum driven winds might contribute to SS 433's mass loss (Clark et al. 2007), they are likely to be of less importance than line-driven winds in this particular case, because of the presence of high velocity outflows ($> 1400 \text{ km s}^{-1}$ see Section 3) with high temperatures, diagnostics which rule out continuum driven winds as main responsible of mass loss.

4.3 The circumbinary ring: near-IR view and mass-loss rate

The idea of the presence of a circumbinary disc in SS 433 was considered by Fabrika (1993) and recently detected by Blundell et al. (2008) by decomposing the H α line profile in three components (during its quiescent state). In the optical this circumbinary ring of material orbits the system at a speed of $\sim 200 \text{ km s}^{-1}$. It has been proposed that the origin of this glowing material corresponds to overflow of gas from the L2 point, assuming that the system has filled its Roche lobe (Fabrika 1993; Blundell et al. 2008; Filippenko et al. 1988). Our Br γ decomposition is in excellent agreement with the presence of this excretion disc since we see a pair of lines, one permanently blueshifted and the other permanently redshifted at fairly stable wavelengths, lacking any orbital phase dependence and rotating at speeds close to 200 km s^{-1} .

4.4 Mass-transfer rates in SS 433 and comparisons with the Eddington rate

According to the basic theory of magneto-hydrodynamic winds from accretion discs, the mass-loss in the wind is about an order of magnitude smaller than the mass accretion rate (inflow at the centre of the disc), i.e., $\dot{M}_{\text{wind}} \simeq 10 \dot{M}_{\text{acc}}$ (Konigl & Pudritz 2000). Based on our estimate of the mass outflow in the wind $\dot{M}_{\text{wind}} = 1 \times 10^{-4} M_{\odot} \text{ yr}^{-1}$, this implies an accretion rate of the order of $\dot{M}_{\text{acc}} \approx 10^{-3} M_{\odot} \text{ yr}^{-1}$. On the other hand, the maximum accretion rate allowed by the Eddington criterion, which assumes spherical symmetry, is $\dot{M}_{\text{acc}} = 4\pi c m_{\text{p}} R_{\text{iso}} / \sigma_{\text{T}}$, where $R_{\text{iso}} = 6GM/c^2$ is the radius of the last stable orbit. This yields a maximum accretion rate of $\dot{M}_{\text{acc}} \simeq 10^{-7} M_{\odot} \text{ yr}^{-1}$ for a black-hole of $16 M_{\odot}$. This is greatly exceeded by our estimate of the accretion rate in the disc, hence confirming the super-Eddington nature of SS 433, which is permitted of course because of the non-spherical geometry of the accretion.

5 CONCLUDING REMARKS

A succession of near-IR spectroscopic observations, taken nightly throughout an entire cycle of SS 433's orbit with UIST on UKIRT, has revealed:

(i) The persistent signature of SS 433's accretion disc as two emission components, blue- and red-shifted, having a rotation speed of $\sim 500 \text{ km s}^{-1}$. The difference in area and in height between each component shows a clear orbital phase dependence, very likely the signature of the disc being eclipsed out as the star transits in front of it. This contributes only about 15 ± 5 per cent of the total Br γ emission line in the near-IR.

(ii) The presence of the circumbinary disc (excretion disc) recently discovered at optical wavelengths by Blundell et al. (2008). It contributes about 15 ± 5 per cent of the total emission in Br γ .

(iii) A much faster outflow than has previously been measured from the wind. What supports the model that the wind comes from the accretion disc is that the luminosity of the broad component attains its maximum at $\phi_{\text{orb}} \sim 0.5$, when the compact object is closer to us (see Section 4.1). The presence of this faster outflow ($v \sim 1500 \text{ km s}^{-1}$) yields a new upper limit for the mass-loss of $\dot{M}_{\text{wind}} = 1 \times 10^{-4} M_{\odot} \text{ yr}^{-1}$. This outflow corresponds to a very significant 70 ± 5 per cent of the total Br γ line emission.

These, together with the newly (upwardly) determined masses for the components of the SS 433 system, result in an accurate diagnosis of the extent to which SS 433 has super-Eddington flows: its accretion rate is 10^4 times higher than the Eddington limit. Our relatively high spectral resolution at these near-IR wavelengths has enabled us to deconstruct the different components, and their physical origins, that comprise the Brackett- γ line in this binary system. With this line dominating throughout our series of observations by the disc wind, and the accretion disc being only a minority ($\lesssim 15$ per cent) contribution, we caution against use of the unresolved Brackett- γ line intensity as an "accretion signature" in X-ray binaries or microquasars in any quantitative way.

ACKNOWLEDGMENTS

We are very grateful to the Sciences and Technology Facilities Council (STFC) studentship for the support of this research. We warmly thank the referee for useful comments on the manuscript. The United Kingdom Infrared Telescope is operated by the Joint Astronomy Centre on behalf of STFC of the U.K. We are especially grateful to the staff of UKIRT especially Paul Hirst for their flexibility and assistance they gave us in the accommodation and execution of our time-resolved observations. K. B. thanks the Royal Society for a University Research Fellowship.

REFERENCES

- Bandyopadhyay, R., Shahbaz, T., Charles, P. A., van Kerkwijk, M. H., & Naylor, T. 1997, MNRAS, 285, 718
- Bandyopadhyay, R. M., Shahbaz, T., Charles, P. A., & Naylor, T. 1999, MNRAS, 306, 417
- Blundell, K. M., & Bowler, M. G. 2004, ApJL, 616, L159
- Blundell, K. M., Bowler, M. G., & Schmidtobreick, L. 2008, ApJ, 678, L47
- Castor, J. I., & Lamers, H. J. G. L. M. 1979, ApJS, 39, 481
- Clark, D. H., & Murdin, P. 1978, Nature, 276, 44
- Clark, J. S., Barnes, A. D., & Charles, P. A. 2007, MNRAS, 380, 263
- Crampton, D., & Hutchings, J. B. 1981, ApJ, 251, 604
- Dhillon, V. S., & Marsh, T. R. 1995, MNRAS, 275, 89
- D'Odorico, S., Oosterloo, T., Zwitter, T., & Calvani, M. 1991, Nature, 353, 329
- Fabian, A. C., & Rees, M. J. 1979, MNRAS, 187, 13P
- Fabrika, S. N. 1993, MNRAS, 261, 241
- Fabrika, S. 2004, Astrophysics and Space Physics Reviews, 12, 1
- Falomo, R., Boksenberg, A., Tanzi, E. G., Tarengi, M., & Treves, A. 1987, MNRAS, 224, 323
- Filippenko, A. V., Romani, R. W., Sargent, W. L. W., & Blandford, R. D. 1988, AJ, 96, 242

- Fuchs, Y., Koch Miramond, L., & Ábrahám, P. 2006, *A&A*, 445, 1041
- Gies, D. R., Huang, W., & McSwain, M. V. 2002, *ApJ*, 578, L67
- Goranskii, V. P., Esipov, V. F., & Cherepashchuk, A. M. 1998, *Astronomy Reports*, 42, 209
- Hillwig, T. C., & Gies, D. R. 2008, *ApJL*, 676, L37
- Ho, L. C., Filippenko, A. V., Sargent, W. L. W., & Peng, C. Y. 1997, *ApJS*, 112, 391
- Horne, K. 1986, *PASP*, 98, 609
- Katz, J. I., Anderson, S. F., Grandi, S. A., & Margon, B. 1982, *ApJ*, 260, 780
- Kemp, J. C., et al. 1986, *ApJ*, 305, 805
- Kogure, T., & Leung, K.-C. 2007, *The Astrophysics of Emission-Line Stars*, by T. Kogure and K.-C. Leung. Berlin: Springer, 2007. ISBN: 978-0-387-34500-0,
- Konigl, A., & Pudritz, R. E. 2000, *Protostars and Planets IV*, 759
- Leitherer, C. 1988, *ApJ*, 326, 356
- Leitherer, C., Chapman, J. M., & Koribalski, B. 1995, *ApJ*, 450, 289
- Lenzorzer, A., Mokiem, M. R., de Koter, A., & Puls, J. 2004, *A&A*, 422, 275
- Lopez, L. A., Marshall, H. L., Canizares, C. R., Schulz, N. S., & Kane, J. F. 2006, *ApJ*, 650, 338
- McAlary, C. W., & McLaren, R. A. 1980, *ApJ*, 240, 853
- Milgrom, M. 1979, *A&A*, 76, L3
- Ramsay Howat, S. K., et al. 2004, *Proc. SPIE*, 5492, 1160
- Shahbaz, T., Bandyopadhyay, R. M., & Charles, P. A. 1999, *A&A*, 346, 82
- Thompson, R. I., Rieke, G. H., Tokunaga, A. T., & Lebofsky, M. J. 1979, *ApJ*, 234, L135

This paper has been typeset from a $\text{T}_{\text{E}}\text{X}/\text{L}^{\text{A}}\text{T}_{\text{E}}\text{X}$ file prepared by the author.